Unsupervised Generative 3D Shape Learning from Natural Images

Anonymous authors
Paper under double-blind review

Figure 1: Samples from our generator trained on the FFHQ dataset at 128×128 resolution. The first column shows random rendered samples. The other columns show the 3D normal map, texture, background and textured 3D shapes for 5 canonical viewpoints in the range of ± 90 degrees.

Abstract

In this paper we present, to the best of our knowledge, the first method to learn a generative model of 3D shapes from natural images in a fully unsupervised way. For example, we do not use any ground truth 3D or 2D annotations, stereo video, and ego-motion during the training. Our approach follows the general strategy of Generative Adversarial Networks, where an image generator network learns to create image samples that are realistic enough to fool a discriminator network into believing that they are natural images. In contrast, in our approach the image generation is split into 2 stages. In the first stage a generator network outputs 3D objects. In the second, a differentiable renderer produces an image of the 3D object from a random viewpoint. The key observation is that a realistic 3D object should yield a realistic rendering from any plausible viewpoint. Thus, by randomizing the choice of the viewpoint our proposed training forces the generator network to learn an interpretable 3D representation disentangled from the viewpoint. In this work, a 3D representation consists of a triangle mesh and a texture map that is used to color the triangle surface by using the UV-mapping technique. We provide analysis of our learning approach, expose its ambiguities and show how to overcome them. Experimentally, we demonstrate that our method can learn realistic 3D shapes of faces by using only the natural images of the FFHQ dataset.

1 Introduction

Generative Adversarial Nets (GAN) (see Goodfellow et al. (2014)) have become the gold standard of generative model over the years. Their capability is demonstrated in many data sets of natural images. These generative models can create sample images that are nearly indistinguishable from real ones. GANs do not need to make assumptions on the data formation other than applying a neural network on a latent noise input. They can also operate in a fully unsupervised way. GANs have strong theoretical foundations since the beginning. Goodfellow et al. (2014) demonstrate that,

under suitable conditions, GANs learn to generate samples with the same probability distribution of samples in the training data set.

However, there is one notable drawback of GANs compared to classical generative models like Gaussian Mixture Models by Xu & Jordan (1996) or Naive Bayes classifiers by McCallum et al. (1998). Classical models are interpretable, but GANs are not. Interpretability is achieved in classical models by making strong assumptions on the data formation process and by using them on interpretable engineered features.

Our work combines the best of both worlds for 3D shape learning. We keep the advantages of GANs: unsupervised training, applicability on real datasets without feature engineering, the theoretical guarantees and simplicity. We also make our representation interpretable, as our generator network provides a 3D mesh as an output, To make the learning possible, we make the assumption that natural images are formed by a differentiable renderer. This renderer produces fake images by taking the 3D mesh, its texture, a background image and a viewpoint as its input. During training a discriminator network is trained against the generator in an adversarial fashion. It tries to classify whether its input is fake or comes from the training dataset.

The key observation is that a valid 3D object should look realistic from multiple viewpoints. This image realism is thus enforced by the GAN training. This idea was first applied for generating 3D shapes in Gadelha et al. (2017). Their pioneering work had several limitations though. It was only applicable to synthetic images, where the background mask is available and produced only black and white images. Our method works on natural images and we do not need silhouettes as supervision signal.

From a theoretical point of view, image realism means that the images lie inside the support of the probability distribution of natural images (see Ledig et al. (2017), where image realism was used for super-resolution). AmbientGAN of Bora et al. (2018) proves that one can recover an underlying latent data distribution, when a known image formation function is applied to the data. This means that our work and that of Gadelha et al. (2017) are special cases of AmbientGAN. However the 3D shape learning task in general does not satisfy an assumption in Bora et al. (2018), which results in ambiguities in the training. We resolve these issues in our paper by using suitable priors.

We summarize our contributions below:

- For the first time, to the best of our knowledge, we provide a procedure to build a generative model that learns explicit 3D representations in an unsupervised way from natural images. We achieve that using a generator network and a renderer trained against a discriminator in a GAN setting. Samples from our model are shown in Figure 1.

- We introduce a novel differentiable renderer, which is a fundamental component to obtain a high-quality generative model. Notably, it is differentiable with respect to the 3D vertex coordinates. The gradients are not approximated, they can be computed exactly even at the object boundaries and in the presence of self-occlusions.

- We analyze our learning setup in terms of the ambiguities in the learning task. These ambiguities might derail the training to undesirable results. We show that these problems can only be solved when one uses labels or prior knowledge on the data distribution. Finally, we provide practical solutions to overcome the problems that originate from the ambiguities.

2 RELATED WORK

Before we discuss prior work, we would like to state clearly what we mean with supervised, unsupervised and weakly supervised learning in this paper. Usually, supervised learning is understood as using annotated data for training, where the annotation was provided by human experts. In some scenarios the annotation comes from the image acquisition setup. Often these approaches are considered unsupervised, because the annotation is not produced by humans. Throughout our paper we consider supervision based on the objective function and its optimization, and not based on the origin of the annotation. To that purpose, we use the notion of the target and training objective. The *target objective* is defined as the function that measures the performance of the trained model f, *i.e.*,

$$\mathcal{L}_{\text{target}}(f) = \mathbb{E}[l_t(f(\mathbf{x}), \mathbf{y})], \tag{1}$$

Table 1: Comparison of prior work. We indicated all supervision signals for the full training process. In case of methods that work on synthetic images with static background we indicated silhouettes as supervision signal.

3D Method	Supervision Signal						3D Representation				Capabilities	
	Images	3DMM	3D	Keypoints	Silhouettes	Viewpoint	Point Cloud	Voxel	Mesh	Texture	View Control	Natural Images
Geng et al. (2019)	✓	✓	✓	✓					✓	✓		✓
Gecer et al. (2019)	✓	✓		✓					✓	✓	✓	✓
Sanyal et al. (2019)		✓		✓					✓	✓	✓	✓
Ranjan et al. (2018)			✓						✓			
Kato & Harada (2019)	✓				✓	✓			✓	✓		
Achlioptas et al. (2018)			✓				✓					
Wu et al. (2016)			✓					✓				✓
Paysan et al. (2009)			✓						✓	✓	✓	✓
Gerig et al. (2018)			✓						✓	✓	✓	✓
Gadelha et al. (2017)					✓		✓				✓	
Henzler et al. (2018)	✓				✓		✓			✓	✓	✓
Henderson & Ferrari (2019)	✓				✓				✓		✓	
This work	✓								✓	✓	✓	✓

where l_t is the loss function, $\mathbf{x}$, $\mathbf{y}$ are the data and labels respectively. The *training objective* is the function that is optimized during the training, They are defined for the supervised, weakly supervised and unsupervised case as

$$\mathcal{L}_{\text{supervised}}(f) = \mathbb{E}[l_s(f(\mathbf{x}), \mathbf{y})], \tag{2}$$
$$\mathcal{L}_{\text{weakly}}(f) = \mathbb{E}[l_w(f(\mathbf{x}), \mathbf{y}_w)], \tag{3}$$
$$\mathcal{L}_{\text{unsupervised}}(f) = \mathbb{E}[l_u(f(\mathbf{x}))], \tag{4}$$

where $\mathbf{y}_w$ denotes a subset of labels and the loss functions l_s, l_w and l_u may be different from l_t. In the case of most supervised tasks (*e.g.* in classification) the target is the same as the training objective (cross-entropy). Another example is monocular depth estimation. In this case, the inputs are monocular images and the model is trained using stereo images. This makes it a weakly supervised method under the definitions above. The GAN training is unsupervised, it has the same target and training objectives (the Jensen-Shannon divergence), and thus even the target objective does not use labels. In Table 1, we show the most relevant prior work with a detailed list of used supervision signals. There, we consider the full training scenario from beginning to end. For example if a method uses a pre-trained network from another previous work in its setup, we consider it supervised if the pre-trained network used additional annotation during its training.

A very successful 3D generative model is the Basel face model introduced by Paysan et al. (2009), which models the 3D shape of faces as a linear combination of base shapes. To create it, classical 3D reconstruction techniques (see Hartley & Zisserman (2003)) and laser scans were used. This model is used in several methods (*e.g.* Geng et al. (2019); Gecer et al. (2019); Sanyal et al. (2019); Sela et al. (2017); Tran et al. (2017); Genova et al. (2018); Tewari et al. (2017)) for 3D reconstruction tasks by regressing its parameters. There are other methods based on GANs, such as those of Wu et al. (2016); Achlioptas et al. (2018), and autoencoders (*e.g.* Ranjan et al. (2018)) that learn 3D representations by directly using 3D as the supervision signal.

The most relevant papers similar to our work are the ones that use differentiable rendering and using randomly sampled viewpoints to enforce image realism. There are GAN based methods by Gadelha et al. (2017); Henzler et al. (2018) and Variational autoencoder based methods by Henderson & Ferrari (2019); Kato & Harada (2019). However, these methods use weak supervision for training as shown in Table 1.

Our method can also be interpreted as a way to disentangle the 3D and the viewpoint factors from images in an unsupervised manner. Reed et al. (2015) used image triplets for the task. They utilized
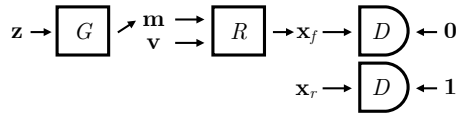
$$\mathbf{z} \to \boxed{G} \nearrow \begin{array}{c} \mathbf{m} \to \\ \mathbf{v} \rightrightarrows \end{array} \to \boxed{R} \to \mathbf{x}_f \to \boxed{D} \!\!\!) \leftarrow 0$$
$$\mathbf{x}_r \to \boxed{D} \!\!\!) \leftarrow 1$$

Figure 2: Illustration of the training setup. G and D are the generator and discriminator neural networks. R is the differentiable renderer and it has no trainable parameters. The random variables $\mathbf{z}$, $\mathbf{m}$ and $\mathbf{v}$ are the latent vector, 3D object and the viewpoint parameters. The fake images are $\mathbf{x}_f$ and the real images are $\mathbf{x}_r$.

an autoencoder to reconstruct an image from the mixed latent encodings of other two images. Mathieu et al. (2016) and Szabó et al. (2018) only use image pairs that share the viewpoint attribute, thus reducing part of the supervision in the GAN training. Similarly, StyleGAN Karras et al. (2019) and Hu et al. (2018) use mixing latent variables for unsupervised disentangling. By using a fixed image formation model, we demonstrate the disentangling of the 3D from the viewpoint without any labels and also guarantee interpretability.

An important component of our model is the renderer. Differentiable renderers like Neural mesh renderer Kato et al. (2018) or OpenDR Loper & Black (2014). have been used along with neural networks for shape learning tasks. Differentiability is essential to make use of the gradient descent algorithms commonly employed in the training of neural networks. We introduce a novel renderer, where the gradients are exactly computed and not approximated at the object boundaries.

3 METHOD

We are interested in building a mapping from a random vector to a 3D object (texture and vertex coordinates), and a background image. We call these three components the *scene representation*. To generate a view of this scene we also need to specify a viewpoint, which we call the *camera representation*. The combination of the scene and camera representations is also referred to as simply the *representation*, and it is used by a differential renderer R to reconstruct an image.

We train a generator G in an adversarial fashion against a discriminator D by feeding zero-mean Gaussian samples $\mathbf{z}_f$ as input (see Fig. 2). The objective of the generator is to map Gaussian samples to scene representations $\mathbf{m}$ that result in realistic renderings $\mathbf{x}_f$ for the viewpoint $\mathbf{v}$ used during training. The discriminator then receives the fake $\mathbf{x}_f$ and real $\mathbf{x}_r$ images as inputs. The GAN training solves the following optimization problem,

$$\min_G \max_D \ \mathbb{E}_{\mathbf{x}_f \sim P_r}[\log(D(\mathbf{x}_f))] + \mathbb{E}_{\mathbf{z} \sim \mathcal{N}, \mathbf{v} \sim P_{\mathbf{v}}}[\log(1 - D(R(G(\mathbf{z}), \mathbf{v})))], \tag{5}$$

where $\mathbf{x}_f = R(G(\mathbf{z}), \mathbf{v})$ are the generated fake images, $\mathbf{m} = G(\mathbf{z})$ are the 3D shape representations and $\mathbf{x}_r$ are the real data samples. The renderer R is a fixed function, *i.e.*, without trainable parameters, but differentiable. The viewpoints $\mathbf{v}$ are randomly sampled from a known viewpoint distribution. In practice, G and D are neural networks and the optimization is done using a variant of Stochastic Gradient Descent (SGD).

4 THEORY

In this section we give a theoretical analysis of our method and describe assumptions that are needed to make the training of the generator succeed. We build on the theory of Bora et al. (2018) and examine its assumptions in the 3D shape learning task.

Assumption 1 *The images in the dataset* $\mathbf{x}_r = R(\mathbf{m}_r, \mathbf{v}_r)$ *are formed by the differentiable rendering function* R *given the 3D representation* $\mathbf{m}_r \sim p_{\mathbf{m}}$ *and* $\mathbf{v}_r \sim p_{\mathbf{v}}$.

Here $p_{\mathbf{m}}$ and $p_{\mathbf{v}}$ are the "true" probability density functions of 3D models and viewpoints. This assumption is needed to make sure that an optimal generator exists. If some real images cannot be generated by the renderer then the generator can never learn the corresponding model. We can safely

assume we have a powerful enough renderer for the task. Note that this does not mean the real data has to be synthetically rendered with the specific renderer R.

Assumption 2 *The ground truth viewpoint $\mathbf{v}_r \sim p_{\mathbf{v}}$ and the 3D models $\mathbf{m}_r \sim p_{\mathbf{m}}$ are independent random variables. The distribution of the 3D representations $p_{\mathbf{m}}$ is not known (it will be learned). The viewpoint distribution $p_{\mathbf{v}}$ is known, and we can sample from it, but the viewpoint $\mathbf{v}_r$ is not known for any specific data sample $\mathbf{x}_r$.*

This assumption is satisfied unless images in the dataset are subject to some capture bias. For example, this would be the case for celebrities that have a "preferred" side of their face when posing for pictures. More technically, this assumption allows us to randomly sample $\mathbf{v}_f$ viewpoints independently from the generated $\mathbf{m}_f$ models.

Assumption 3 *Given the image formation model $\mathbf{x} = R(\mathbf{m}, \mathbf{v})$, when $\mathbf{v} \sim p_{\mathbf{v}}$, there is a unique distribution $p_{\mathbf{m}}$ that induces the data $\mathbf{x} \sim p_{\mathbf{x}}$.*

This assumption is necessary for learning the ground truth $p_{\mathbf{m}}$. In the unsupervised learning task we can only measure the success of the learning algorithm on the output images. If multiple distributions can induce the same data $\mathbf{x} \sim p_{\mathbf{x}}$, there is no way for any learning algorithm to choose between them, unless prior knowledge on $p_{\mathbf{m}}$ (in practice it is an added constrain on $\mathbf{m}$ in the optimization) is available.

The 3D shape learning task in general is ambiguous. For example in the case of the hollow-mask illusion (see Gregory (1970)) people are fooled by an inverted dept image. Many of these ambiguities depend on the parametrization of the 3D representation. For example a mesh can reproduce the same depth image with different triangle configurations, thus it is more ambiguous than a depth map. However, if the aim is to reconstruct the depth of an object, the ambiguities arising from the mesh representation do not cause an ambiguity in the depth. We call these *acceptable ambiguities*.

For natural images one has to model the whole 3D scene, otherwise there is a trivial ambiguity when a static background is used. The generator can simply move the object out of the camera field of view and generate the images on the background like in the GAN training to generate natural images. Modeling the whole scene with a triangle mesh however is problematic in practice because of the large size of the (multiple) meshes that would be needed. We propose a compromise, where we only model the object with the mesh and we generate a large background and crop a portion of it randomly during training. In this way, even if the generator outputs background images with a view of the object, there is no guarantee that the background crop will still contain the object. Thus, the generator will not be able to match the statistics of real data unless it produces a realistic 3D model.

Assumption 4 *The generator G and discriminator D have large enough capacity, and the training reaches the global optimum of the GAN training 5.*

In practice, neural networks have finite capacity and we train them with a local iterative minimization solver (stochastic gradient descent). Hence, the global optimum might not be achieved. Nonetheless we show that the procedure works in practice.

Now we show that under these conditions the generator can learn the 3D geometry of the scene faithfully.

Theorem 1 *When the above assumptions are satisfied, the generated scene representation distribution is identical to the real one, thus $G(\mathbf{z}) \sim p_{\mathbf{m}}$, with $\mathbf{z} \sim \mathcal{N}(0, I)$.*

The proof can be readily adapted from Bora et al. (2018).

5 DIFFERENTIABLE RENDERER

Differentiability is essential for functions used in neural network training. Unfortunately traditional polygon renderers are only differentiable with respect to the texture values but not for the 3D vertex coordinates. When the mesh is shifted by a small amount, the rendered pixel can shift to the background or to another triangle in the mesh. This can cause problems during training. Thus, we propose a novel renderer that is differentiable with respect to the 3D vertex coordinates.

We make the renderer differentiable by extending the triangles at their boundaries with a fixed amount in pixel space. Then, we blend the extension against the background or against an occluded triangle. The rendering is done in two stages. First, we render an image with what we call a *crisp* renderer. Second, we render the triangle extensions and its alpha map, which we call the *soft* image. Finally we blend the crisp and the soft images.

We render the crisp layer using the barycentric coordinates. Let us define the distance of a 2D pixel coordinate $\boldsymbol{p}$ to a triangle T as $d(\boldsymbol{p}, T) = \min_{\boldsymbol{p}_t \in T} d(\boldsymbol{p}, \boldsymbol{p}_t)$ and its closest point in the triangle as $\boldsymbol{p}^*(T) = \arg\min_{\boldsymbol{p}_t \in T} d(\boldsymbol{p}, \boldsymbol{p}_t)$, where d is the Euclidean distance. For each pixel and triangle the rendered attribute and depth, attribute and alpha map can be computed as

$$z_c(\boldsymbol{p}, T) = \mathbf{1}\{d(\boldsymbol{p}, T) = 0\} \sum_{i=1}^{3} b_i(\boldsymbol{p}, T) z_i(T) + (1 - \mathbf{1}\{d(\boldsymbol{p}, T) = 0\}) z_{far} \tag{6}$$

$$a_c(\boldsymbol{p}) = \mathbf{1}\{z_c(\boldsymbol{p}, T^*(\boldsymbol{p})) < z_{far})\} \sum_{i=1}^{3} b_i(\boldsymbol{p}, T) a_i(T_c^*(\boldsymbol{p})) \tag{7}$$

$$\alpha_c(\boldsymbol{p}) = \mathbf{1}\{z_c(\boldsymbol{p}, T^*(\boldsymbol{p})) < z_{far})\} \tag{8}$$

where z_c indicates the crisp layer, b_i are the barycentric coordinates and $z_i(T)$ are the depth values of the triangle vertices and z_{far} is a large number representing infinity. The vertex attributes of a triangle T are $a_i(T)$. The closest triangle index is computed as $T_c^*(\boldsymbol{p}) = \arg\min_T z_c(\boldsymbol{p}, T)$, and it determines which triangle is rendered for the attribute $a_c(\boldsymbol{p})$ crisp image. The soft image is computed as

$$z_s(\boldsymbol{p}, T) = \mathbf{1}\{0 < d(\boldsymbol{p}, T) < B\} \sum_{i=1}^{3} b_i(\boldsymbol{p}^*(T), T) z_i(T) + \tag{9}$$
$$(1 - \mathbf{1}\{0 < d(\boldsymbol{p}, T) < B\}) z_{far} + \lambda_{slope} d(\boldsymbol{p}, T)$$

$$a_s(\boldsymbol{p}) = \frac{\sum_T \mathbf{1}\{z_s(\boldsymbol{p}, T) < z_c(\boldsymbol{p}, T^*(\boldsymbol{p})) \sum_{i=1}^{3} b_i(\boldsymbol{p}^*(T), T) z_i(T)\}}{\sum_T \mathbf{1}\{z_s(\boldsymbol{p}, T) < z_c(\boldsymbol{p}, T^*(\boldsymbol{p}))\}} \tag{10}$$

$$\alpha_s(\boldsymbol{p}) = \max_T \mathbf{1}\{z_s(\boldsymbol{p}, T) < z_c(\boldsymbol{p}, T^*(\boldsymbol{p}))\} d(\boldsymbol{p}, T)/B, \tag{11}$$

where B is the width of the extension around the triangle. The final image $a(\boldsymbol{p})$ is computed as

$$a(\boldsymbol{p}) = \alpha_s(\boldsymbol{p}) a_s(\boldsymbol{p}) + (1 - \alpha_s(\boldsymbol{p})) \alpha_c(\boldsymbol{p}) a_c(\boldsymbol{p}) + (1 - \alpha_c(\boldsymbol{p})) \text{bcg}(\boldsymbol{p}), \tag{12}$$

where bcg is the background crop. UV mapping is supported as well: first the UV coordinates are rendered for the crisp and soft image. Then the colors are sampled from the texture map for the soft and the crisp image separately. Finally, the soft and the crisp images are blended. Figure 3 shows an illustration of the blended rendering as well as its effect on the training.

6   3D REPRESENTATION

The 3D representation $\mathbf{m} = [\mathbf{s}, \mathbf{t}, \mathbf{b}]$ consists of three parts, where $\mathbf{s}$ denotes the 3D shape of the object, $\mathbf{t}$ are the texture and $\mathbf{b}$ are the background colour values.

The shape $\mathbf{s}$ is a 3 dimensional array with the size of $3 \times N \times N$. We call this the shape image, where each pixel corresponds to a vertex in our 3D mesh and the pixel value determines the 3D coordinates of the vertex. The triangles are defined as the subset of the regular triangular mesh on the $N \times N$ grid; we only keep the triangles of the middle circular region. The texture (image) is an array of the size $3 \times N_t \times N_t$. The renderer uses the UV mapping technique, so the size of the texture image can have higher resolution than the shape image. In practice we choose $N_t = 2 \times N$, so the triangles are roughly 1 or 2 pixels wide and the texture can match the image resolution when rendering a $N \times N$ image. The background is a color image of size $3 \times 2N \times 2N$

The renderer uses a perspective camera model, where the camera is pointing at the origin and placed along the Z axis such that the field of view is set so the unit ball fits tightly in the image. The viewpoint change is interpreted as rotating the object in 3D space, while the camera stays still. Finally a random $N \times N$ section of the renderer is cropped and put behind the object.

Notice that the 3D representation (3 dimensional arrays) are a perfect match for convolutional neural network generators. We designed it this way, so we can use StyleGAN as generator (see Karras et al. (2019)).

7 Network Architecture

We use the StyleGAN generator of Karras et al. (2019) with almost vanilla settings to generate the shape image, texture image and the background. StyleGAN consist of two networks: an 8 layer fully connected mapping network that produces a style vector from the latent inputs, and a synthesis network that consist of convolutional and upsampling layers that produces the output image. The input of the synthesis network is constant and the activations at each layer are perturbed by the style vector using adaptive instance normalization. For each layer activation also noise is added. It is also possible to mix styles from different latent vectors, by perturbing the convolutional layer activations with different styles at each layer. In our work we used the default setting for style mixing and for most parameters. We modified the number of output channels, the resolution and learning rates. The training was done in a progressively growing fashion, starting at the an image resolution of 16×16. The final resolution was set to 128×128.

One StyleGAN instance (G_o) generates the shape image and texture and another (G_b) generates the background. The inputs to both generators are 512 dimensional latent vectors $\mathbf{z}_o$ and $\mathbf{z}_b$. We sampled them independently, assuming the background and the object are independent. We set both G_o and G_b to produce images at $2N \times 2N$ resolution where N is the rendered image size. The output of the object generator is then sliced into the shape and texture image, then the texture image is downsampled by a factor of 2.

We noticed that during the training the generation of shapes would not easily recover from bad local minima, which resulted in high frequency artifacts and the hollow-mask ambiguity. Thus we use a shape image pyramid to tackle this problem. The generator is set to produce $K = 4$ shape images, then these images are blurred with varying amounts and summed:

$$\mathbf{s}_{pyr} = \sum_{k=0}^{K-1} \frac{\text{blur}(\mathbf{s}_i, \sigma = 2^k)}{2^k}, \tag{13}$$

where $\text{blur}(\cdot)$ is the Gaussian blur and σ is interpreted in pixels on the shape image.

We also noticed that the 3D models of the object tended to grow large and tried to model the background. This is the result of an acceptable ambiguity in the parametrization, In terms of the GAN objective it does not matter if the background is modelled by $\mathbf{b}$ or $\mathbf{s}$ and $\mathbf{t}$. As we are interested in results where the object fits in the image, we added a size constraint on the object. The output coordinates are computed as

$$\mathbf{s}_{size} = \mathbf{s}\frac{\tanh(|\mathbf{s}|)}{|\mathbf{s}|}s_{max}, \tag{14}$$

where we set $s_{max} = 1.3$ and the L^2 norm and $\tanh$ functions are interpreted pixel-wise on the shape image $\mathbf{s}$. The effect of bot the shape image pyramid and the size constraint can be seen in Figure 3.

8 Experiments

We trained our model on the FFHQ dataset (Karras et al., 2019). It contains 70k images high resolution 1024×1024 colour images. We resized the images to 128×128 and trained our generative model on all images in the dataset. For the viewpoint we found that randomly rotating in the range of ± 45 degrees along the vertical and ± 15 degrees along the horizontal axis yielded the best results. This is not surprising, as most faces in the dataset are close to frontal. Except for Figure 3, we used pyramid shapes of 4 levels and size constraint of 1.3. We trained our model for 5M iterations.

First we show ablations of the choices of the renderer and network architecture setting on Figure 3. The first image shows an illustration of the soft renderer that is used in the training. The following figures show training with different settings. We can see that our soft renderer has a large impact on the training. The crisp renderer cannot learn the shape. Furthermore we can see that the size constraint prevents the mesh to model the background, and the shape pyramid reduces the artifacts and folds on the face. We can also see that it is important that we set the viewpoint distribution accurately. With the a large viewpoint range ± 120 degrees our method struggles to learn. It puts multiple faces on the object.
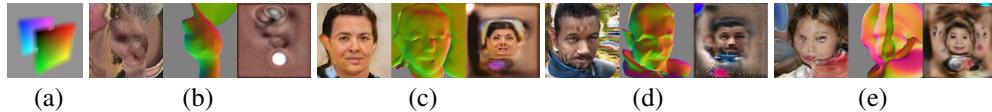
| (a) | (b) | (c) | (d) | (e) |

Figure 3: a) illustration of the soft renderer; b) results with crisp renderer; c) results with soft renderer; d) results with soft renderer + size constraint; e) results with soft renderer + size constraint + pyramid on viewpoint range of ± 120 degrees.
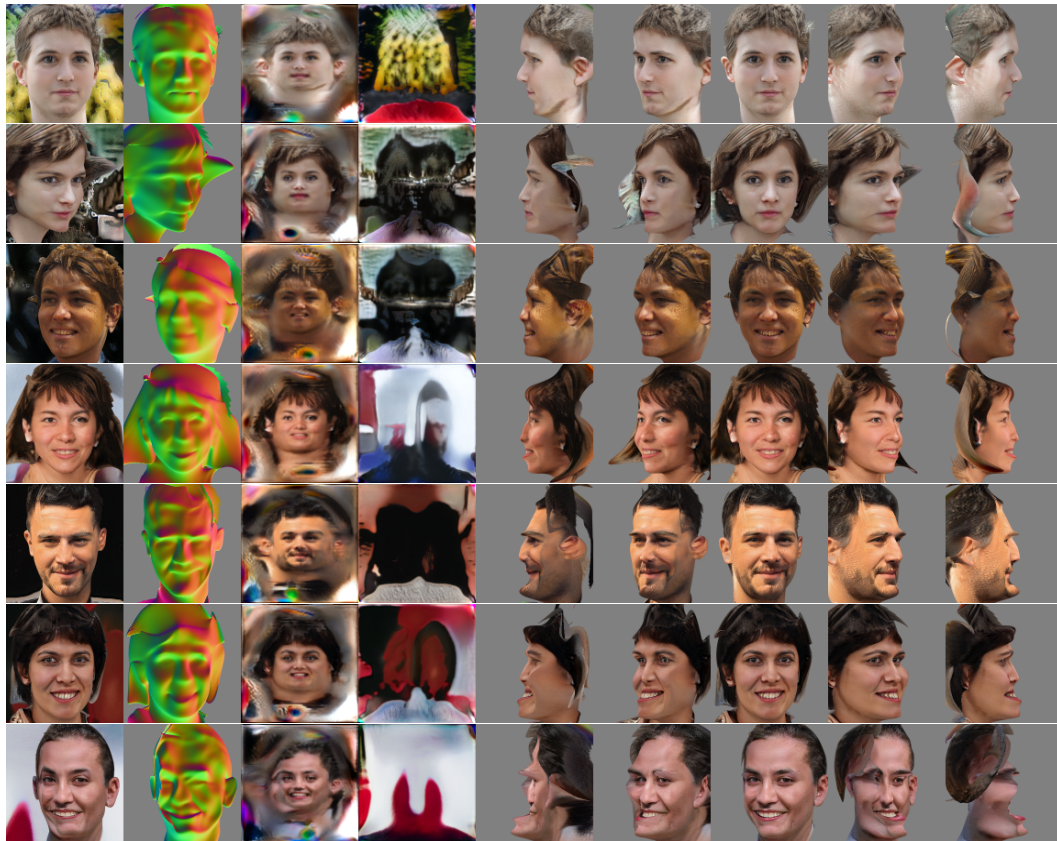

Figure 4: Samples from our generator trained on the FFHQ dataset at 128×128 resolution. The first column shows random rendered samples. The other columns show the 3D normal map, texture, background and textured 3D shapes for 5 canonical viewpoints in the range of ± 90 degrees.

In Figure 4 we can see samples from our generator. The images were picked to illustrate the range of quality achieved by our method. We can see that most of the samples have anatomically correct shapes. In some cases there are exaggerated features like a large chin, that is only apparent from the profile view. Faces from those viewpoints are not present in the dataset, which might explain the shortcomings of our method. There are failure cases as well (the bottom row), that looks realistic from the frontal view, but does not look like a face from the side. More random samples can be found in the Appendix.

Figure 5 shows results on interpolated features. We can see the viewpoint and the identity is disentangled and the transition is smooth.

9 DISCUSSION

Here, we would like to acknowledge the limitations of our work:

Figure 5: Interpolated 3D models. From top to bottom the 3D models are generated by linearly interpolating the latent vector fed to the generator. We show 3 viewpoint in the range of ± 45 degrees

- Currently, we use a triangle mesh with fixed topology. In general, this is not sufficient for modeling challenging objects and scenes of arbitrary topology.

- The background is currently not modeled as part of the triangle mesh, which limits our method for datasets where the object is found at the center of the image. Note that this limitation is the result of the specific parametrization and the architecture of the generator and not of the expressive power of our method in general.

- The imaging model is currently Lambertian. However, specularity and illumination can be added to the renderer model. This is a relatively simple extension, but the representation of lights as random variables during training needs extensive experimental evaluation.

One might claim that our work does use supervision, as the faces FFHQ dataset were carefully aligned to the center of the images. We argue that our method still does not use any explicit supervision signal other than the images themselves. Moreover, as discussed in the limitation section, the centering of the object will be irrelevant when the background and the object share the same 3D mesh and texture. In contrast, methods that use annotation cannot be extended to deal with more challenging datasets, where that annotation is not available.

Another point is the motivation to generate faces in an unsupervised manner, since there already exist several data sets with lots of annotation. First, we choose FFHQ because it is a very clean dataset and our intention is to demonstrate that unsupervised 3D shape learning is possible. Second, we believe that unsupervised learning is the right thing to do even if annotation is available. Unsupervised methods can be extended to other datasets where that annotation is not available.

In conclusion, we provide a solution to the challenging and fundamental problem of building a generative model of 3D shapes in an unsupervised way. We explore the ambiguities present in this task and provide remedies for them. Our analysis highlights the limitations of our approach and sets the direction for future work.

REFERENCES

Panos Achlioptas, Olga Diamanti, Ioannis Mitliagkas, and Leonidas Guibas. Learning representations and generative models for 3d point clouds, 2018. URL https://openreview.net/forum?id=BJInEZsTb.

Ashish Bora, Eric Price, and Alexandros G. Dimakis. AmbientGAN: Generative models from lossy measurements. In *ICLR*, 2018.

Matheus Gadelha, Subhransu Maji, and Rui Wang. 3d shape induction from 2d views of multiple objects. In *International Conference on 3D Vision*, 2017.

Baris Gecer, Stylianos Ploumpis, Irene Kotsia, and Stefanos Zafeiriou. Ganfit: Generative adversarial network fitting for high fidelity 3d face reconstruction. In *The IEEE Conference on Computer Vision and Pattern Recognition (CVPR)*, June 2019.

Zhenglin Geng, Chen Cao, and Sergey Tulyakov. 3d guided fine-grained face manipulation. In *The IEEE Conference on Computer Vision and Pattern Recognition (CVPR)*, June 2019.

Kyle Genova, Forrester Cole, Aaron Maschinot, Aaron Sarna, Daniel Vlasic, and William T Freeman. Unsupervised training for 3d morphable model regression. In *CVPR*, 2018.

Thomas Gerig, Andreas Morel-Forster, Clemens Blumer, Bernhard Egger, Marcel Luthi, Sandro Schönborn, and Thomas Vetter. Morphable face models-an open framework. In *Automatic Face & Gesture Recognition*. IEEE, 2018.

Ian Goodfellow, Jean Pouget-Abadie, Mehdi Mirza, Bing Xu, David Warde-Farley, Sherjil Ozair, Aaron Courville, and Yoshua Bengio. Generative adversarial nets. In *NIPS*, 2014.

R. L Gregory. *The intelligent eye*. Weidenfeld & Nicolson, 1970. ISBN 0297000217. URL https://www.amazon.com/intelligent-eye-R-L-Gregory/dp/0297000217?SubscriptionId=AKIAIOBINVZYXZQZ2U3A&tag=chimbori05-20&linkCode=xm2&camp=2025&creative=165953&creativeASIN=0297000217.

Richard Hartley and Andrew Zisserman. *Multiple view geometry in computer vision*. Cambridge university press, 2003.

Paul Henderson and Vittorio Ferrari. Learning single-image 3d reconstruction by generative modelling of shape, pose and shading. *CoRR*, abs/1901.06447, 2019. URL http://arxiv.org/abs/1901.06447.

Philipp Henzler, Niloy J. Mitra, and Tobias Ritschel. Escaping plato's cave using adversarial training: 3d shape from unstructured 2d image collections. *CoRR*, abs/1811.11606, 2018. URL http://arxiv.org/abs/1811.11606.

Qiyang Hu, Attila Szabó, Tiziano Portenier, Paolo Favaro, and Matthias Zwicker. Disentangling factors of variation by mixing them. In *CVPR*, 2018.

Tero Karras, Samuli Laine, and Timo Aila. A style-based generator architecture for generative adversarial networks. In *Proceedings of the IEEE Conference on Computer Vision and Pattern Recognition*, pp. 4401–4410, 2019.

Hiroharu Kato and Tatsuya Harada. Learning view priors for single-view 3d reconstruction. In *The IEEE Conference on Computer Vision and Pattern Recognition (CVPR)*, June 2019.

Hiroharu Kato, Yoshitaka Ushiku, and Tatsuya Harada. Neural 3d mesh renderer. In *CVPR*, 2018.

Christian Ledig, Lucas Theis, Ferenc Huszár, Jose Caballero, Andrew Cunningham, Alejandro Acosta, Andrew Aitken, Alykhan Tejani, Johannes Totz, Zehan Wang, et al. Photo-realistic single image super-resolution using a generative adversarial network. In *Proceedings of the IEEE conference on computer vision and pattern recognition*, pp. 4681–4690, 2017.

Matthew M Loper and Michael J Black. Opendr: An approximate differentiable renderer. In *ECCV*, 2014.

Michael F Mathieu, Junbo Jake Zhao, Junbo Zhao, Aditya Ramesh, Pablo Sprechmann, and Yann LeCun. Disentangling factors of variation in deep representation using adversarial training. In *NIPS*, 2016.

Andrew McCallum, Kamal Nigam, et al. A comparison of event models for naive bayes text classification. In *AAAI-98 workshop on learning for text categorization*, volume 752, pp. 41–48. Citeseer, 1998.

Pascal Paysan, Reinhard Knothe, Brian Amberg, Sami Romdhani, and Thomas Vetter. A 3d face model for pose and illumination invariant face recognition. In *Advanced video and signal based surveillance*, 2009.

Anurag Ranjan, Timo Bolkart, Soubhik Sanyal, and Michael J. Black. Generating 3d faces using convolutional mesh autoencoders. In *The European Conference on Computer Vision (ECCV)*, September 2018.

Scott E Reed, Yi Zhang, Yuting Zhang, and Honglak Lee. Deep visual analogy-making. In *Advances in neural information processing systems*, 2015.

Soubhik Sanyal, Timo Bolkart, Haiwen Feng, and Michael J. Black. Learning to regress 3d face shape and expression from an image without 3d supervision. In *The IEEE Conference on Computer Vision and Pattern Recognition (CVPR)*, June 2019.

Matan Sela, Elad Richardson, and Ron Kimmel. Unrestricted facial geometry reconstruction using image-to-image translation. In *ICCV*, 2017.

Attila Szabó, Qiyang Hu, Tiziano Portenier, Matthias Zwicker, and Paolo Favaro. Understanding degeneracies and ambiguities in attribute transfer. In *ECCV*, 2018.

Ayush Tewari, Michael Zollhöfer, Hyeongwoo Kim, Pablo Garrido, Florian Bernard, Patrick Pérez, and Christian Theobalt. Mofa: Model-based deep convolutional face autoencoder for unsupervised monocular reconstruction. In *ICCV*, 2017.

Anh Tuan Tran, Tal Hassner, Iacopo Masi, and Gérard Medioni. Regressing robust and discriminative 3d morphable models with a very deep neural network. In *CVPR*, 2017.

Jiajun Wu, Chengkai Zhang, Tianfan Xue, Bill Freeman, and Josh Tenenbaum. Learning a probabilistic latent space of object shapes via 3d generative-adversarial modeling. In D. D. Lee, M. Sugiyama, U. V. Luxburg, I. Guyon, and R. Garnett (eds.), *Advances in Neural Information Processing Systems 29*, pp. 82–90. Curran Associates, Inc., 2016.

Lei Xu and Michael I Jordan. On convergence properties of the em algorithm for gaussian mixtures. *Neural computation*, 8(1):129–151, 1996.

A APPENDIX

Figure 6: Random samples from our generator. The format is the same as in Figure 1.